Journal of Membrane Science 618 (2021) 118745

Contents lists available at ScienceDirect

Journal of Membrane Science

journal homepage: http://www.elsevier.com/locate/memsci

Centimeter-scale gas-sieving nanoporous single-layer graphene membrane

Wan-Chi Lee, Luc Bondaz, Shiqi Huang, Guangwei He, Mostapha Dakhchoune, Kumar Varoon Agrawal *

Laboratory of Advanced Separations, École Polytechnique Fédérale de Lausanne, Sion, Switzerland

ARTICLE INFO

Keywords:
Single-layer graphene
Gas separation
Molecular sieving
Mechanical reinforcement
Scale-up

ABSTRACT

High-permeance, molecular-sieving, nanoporous single-layer graphene (NSLG) membranes are highly promising for gas separation. However, the formation of cracks during the transfer of NSLG to a low-cost porous support is difficult to avoid. These cracks are detrimental to gas selectivity, and therefore, make the scale-up of the gas-sieving NSLG membranes challenging. To mitigate the crack formation on low-cost macroporous supports, herein, we demonstrate mechanical reinforcement of the graphene film with a two-layer composite carbon film. The bottom layer of the composite film is a 100-nm-thick block-copolymer film derived nanoporous carbon (NPC) film with a pore size of 20–30 nm. This layer makes an intimate contact with NSLG and prevents generation of crack. However, the NPC film by itself is not robust enough to cover the rough surface of low-cost macroporous supports and tends to generate occasional cracks. This is prevented by spin-coating a 500-nm-thick multi-walled carbon nanotube (MWNT) film, hosting pore size of 200–300 nm, on top of the NPC film. This imparts enough mechanical strength to NSLG/NPC film to be successfully suspended on a low-cost, macroporous, nonwoven metal wire mesh on a centimeter-scale while completely avoiding cracks. As a result, H_2/CH_4 and H_2/CO_2 selectivities of 11–23 and 5–8, respectively, higher than the corresponding Knudsen selectivities of 2.8 and 4.7, respectively, are obtained from the centimeter-scale NSLG membranes. The reinforced membranes are mechanically robust and can successfully withstand transmembrane pressure difference of 4 bar. When the MWNT film is directly coated on NSLG without using the intermediate NPC layer, the gas sieving behavior is not observed, likely due to the development of nanoscale cracks. This underlines the crucial role of the hierarchical pore structure in the composite carbon film in realizing the gas-sieving graphene membranes.

1. Introduction

Atom-thick single-layer graphene (SLG) film incorporated with sub-nanometer pores enables high-flux yet selective molecular transport, and is promising for improving the energy-efficiency of water desalination [1–5] and gas separation [6–14]. However, a key bottleneck in the scale-up of nanoporous SLG (NSLG) membranes, especially for the gas separation, is the fabrication of large-area NSLG films without cracks and tears on low-cost porous supports. This is because the gas transport from a nanoscale crack in NSLG is several orders of magnitude faster than that from a molecular-sieving nanopore [15]. For example, the permeation coefficients of H_2 and CH_4 from a large non-selective defect (e.g. 2–50 nm in size) are within the same order of magnitude, ca. 10^{-18}–10^{-19} mol s^{-1} Pa^{-1} [16,17]. In comparison, the permeation coefficient of H_2 from a H_2-selective nanopore is much smaller, in the range of 10^{-21} to 10^{-22} mol s^{-1} Pa^{-1} [10]. The permeation coefficient of CH_4 from a H_2-selective nanopore, assuming H_2/CH_4 selectivity of 100–1000, is even smaller, lower than 10^{-24} [10]. As such, even a few ppm of nanoscale cracks in NSLG will significantly increase CH_4 transport, deteriorating the gas selectivity.

The cracks and tears in the suspended graphene film originate during the transfer of graphene onto a porous support. The fabrication of NSLG-based membranes involves three key steps, (i) synthesis of SLG, (ii) incorporation of gas-selective nanopores in SLG and (iii) transfer of NSLG to a porous support. High-quality SLG with a low density of intrinsic defects is synthesized by chemical vapor deposition (CVD) of a hydrocarbon precursor on a Cu foil, a process that has been demonstrated on a scalable roll-to-roll basis [2,18]. Since the pristine graphene lattice is theoretically impermeable to molecules, molecular-selective nanopores with a narrow pore-size-distribution (PSD) in SLG are introduced by chemical or physical etching techniques [19,20]. Finally, NSLG is transferred from the Cu foil to the target porous support. It is

* Corresponding author.
E-mail address: kumar.agrawal@epfl.ch (K.V. Agrawal).

https://doi.org/10.1016/j.memsci.2020.118745
Received 3 August 2020; Received in revised form 10 September 2020; Accepted 11 September 2020
Available online 16 September 2020

this transfer step that leads to mechanical-stress-induced cracks and tears in the NSLG film [21–23]. Therefore, it is essential to provide mechanical reinforcement to the NSLG membrane, which at the same time helps to fulfill the requirement of membrane-based gas separation i.e., pressurization [24]. A strategy to achieve this is to integrate NSLG with a mechanically-reinforcing porous film that does not restrict the molecular transport across graphene. Naturally, the conventional and most popular poly(methyl methacrylate) (PMMA) [25] reinforcement of graphene is ruled out because PMMA has a small gas permeability and, therefore, would control the overall gas transport. In this regard, one can use a porous polymer film as the reinforcement. For example, a porous polymer film can be directly cast on top of graphene by the non-solvent induced phase separation (NIPS) process [12,23]. However, in this method, graphene contacts the bottom layer of the polymer film, and the presence of macrovoids or micron-sized pores in the bottom layer of the polymer film does not provide sufficient mechanical reinforcement, and cracks in the suspended graphene film develop during the NIPS process. We recently reported hydrogen-sieving NSLG membranes with 1 mm^2 area, using a block-copolymer-templated nanoporous carbon (NPC) film to reinforce graphene, with the resolution of molecular differentiation approaching 1 Å [8,9]. However, these membranes were fabricated on laser-drilled smooth tungsten foils which are difficult to scale up [26]. As we show here, the standalone NPC film tends to develop cracks when transferred onto low-cost macroporous supports which generally have a relatively higher surface roughness compared to the tungsten foil. Recently, Yang and co-workers demonstrated a centimeter-sized single-walled carbon nanotube (SWNT) reinforced, crack-free NSLG membranes for nanofiltration, achieving Na^+ and Rhodamine B rejections of 85 and 97%, respectively [3]. Such reinforcement also allowed the construction of tubular water-desalination modules, yielding salt rejection up to 95.3%. Nevertheless, it is unclear that this method would lead to gas-sieving membranes because molecular diffusivity in the gas phase is four to five orders of magnitude larger than that in the liquid phase. Further, the size differences between the gas molecules are much smaller than those between water and hydrated ions. As we show later, we could not obtain a gas-sieving performance from graphene supported by a carbon nanotube mesh.

Herein, we report a method to fabricate centimeter-scale gas-sieving NSLG membranes on a commercial low-cost stainless-steel nonwoven mesh (pore size of 20 μm) where the mechanical reinforcement is provided from a two-layer composite carbon film. The bottom layer of the reinforcement is composed of a 100-nm-thick NPC film while the top layer is made up of a 500-nm-thick multi-walled carbon nanotubes (MWNT) film with a pore size in the film ranging from 200 to 300 nm. The NPC film has a high affinity with graphene lattice while MWNT film is mechanically robust, and improves the overall mechanical robustness of the composite film. As a result, centimeter-scale film could be prepared on low-cost macroporous support. The resulting films could withstand pressurization, and yielded attractive H_2/CH_4 and H_2/CO_2 selectivities of 11–23 and 5–8, respectively, significantly higher than the corresponding Knudsen selectivities.

2. Experimental

2.1. Synthesis of SLG by low-pressure chemical vapor deposition (LPCVD)

SLG was synthesized by the LPCVD process using a Cu foil (25 μm thick, 99.98% purity, Alfa-Aesar or 50 μm thick, 99.9% purity, Strem) as a catalytic substrate. Briefly, the Cu foil was subjected to CO_2 and H_2 annealing at 1000 °C for 30 min, respectively. Afterward, CH_4 (24 sccm) and H_2 (8 sccm) were introduced into the reactor at a total pressure of 460 mtorr for 30 min for the nucleation and growth of the polycrystalline SLG film. The quartz tube used as the LPCVD reactor was subsequently pulled out from the hot furnace at the end of the synthesis to rapidly quench the crystallization. The as-synthesized graphene was either directly used to fabricate membranes or was further treated by ozone to incorporate the gas-selective nanopores.

2.2. Fabrication of graphene/NPC/MWNT membranes

Nanopores in single-layer graphene were introduced by exposing as-synthesized graphene on Cu to a short ozone (9% in O_2) pulse at 250 °C (pulse FWHM < 0.3 s) [9]. The reinforcing layer of the graphene membrane was made by the deposition of an NPC film followed by the deposition of an MWNT film on top of the NPC film. The fabrication of the NPC film was similar to the procedure reported elsewhere [8]. Briefly, the precursor of NPC was prepared by dissolving 0.1 g block-copolymer (poly (styrene-b-4-vinyl pyridine), Polymer Source) and 0.2 g turanose (Sigma Aldrich) in dimethylformamide (Sigma Aldrich) followed by heat treatment of the solution at 180 °C. The solution was spin-coated on the graphene film and pyrolyzed at 500 °C in a H_2 (15 sccm)/Ar (200 sccm) atmosphere, with a total pressure of 1 bar for 1 h to yield the NPC film. It has a mix of somewhat interconnected as well as straight pore channels where the proportional is determined by the annealing of the block copolymer film. It hosts a pore size of 20–30 nm, which corresponds to a density of 10^{-3} nm^{-2} for the pores opening to the top surface. The MWNT coating suspension was prepared by dispersing MWNT powders (multi-walled, carboxylic acid functionalized, average diameter and length of 9.5 and 1500 nm, respectively, Sigma Aldrich) with surfactant (modified polyvinyl alcohol, XFNano, China) in dimethylformamide (Sigma Aldrich) at a weight ratio of 2:1. Following this, the suspension was sonicated for 3 h to obtain a uniform dispersion (average length of 690 nm after the sonication). The MWNT film was deposited by spin-coating 0.5 mL of pre-dispersed suspension on top of the NPC reinforced graphene film at a spin speed of 1500 rpm for 1 min. After the deposition, the sample was pyrolyzed at 500 °C in a H_2/Ar atmosphere for 1 h. The resulting composite film was floated on a $Na_2S_2O_8$ bath (0.2 M in water) to etch the Cu foil. After Cu etching, the floating film was transferred to a deionized water bath to rinse the backside of the film. Finally, the rinsed film floating on water was scooped by a polished stainless-steel mesh (pore size 20 μm, TWP Inc., Part number #325X2300TL0014).

2.3. Characterization

Scanning electron microscope (SEM) images were obtained by using FEI Teneo scanning electron microscope at 1.0–5.0 kV and working distances of 2.5–5.0 mm. No conductive coating was applied to the substrates before SEM. Transmission electron microscope (TEM) imaging and selected area electron diffraction (SAED) of the composite graphene film were conducted by FEI Tecnai G2 Spirit Twin transmission electron microscope with a 120 kV incident electron beam. Raman measurement was carried on graphene on a Cu foil right after the synthesis and pore etching using 457 nm excitation or on graphene transferred to a Si/SiO_2 wafer using 532 nm excitation using Renishaw micro-Raman spectroscope with 100× objective. The obtained Raman data was analyzed using a MATLAB script. For the calculation of the D and the G peak height, the background was subtracted from the Raman data using the least-squares curve fitting tool (lsqnonlin).

2.4. Gas permeation test

The single-component and mixed-gas permeation tests were carried out in a homemade permeation cell reported elsewhere [27]. The mass flow controllers (MKS and Brooks Instruments) were pre-calibrated using a bubble flow meter, delivering a pre-determined amount of gas to the feed side. The transmembrane pressure difference was varied between 1 and 4 bar with the permeate side maintained at 1 bar using an Ar sweep. The permeate was connected to a pre-calibrated mass spectrometer allowing real-time analysis of the permeate gas. The graphene membranes were sealed on to an annular metal disk using an

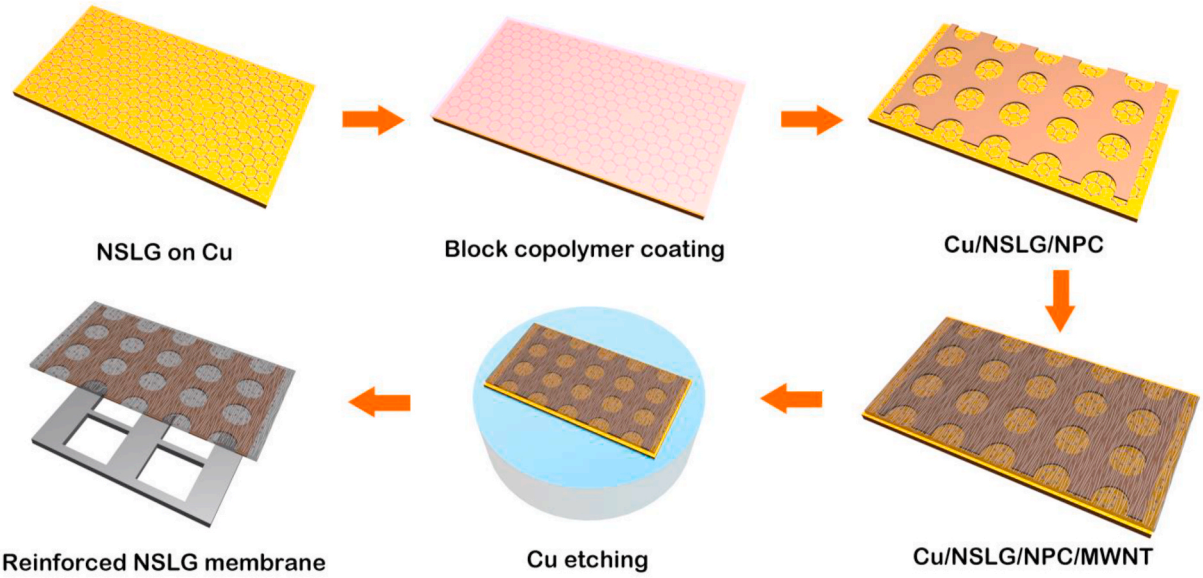

Fig. 1. Schematic of the fabrication of large-area NSLG membranes using the composite NPC/MWNT film as a reinforcing layer. Briefly, a block-copolymer/turanose solution was coated on the NSLG film resting on a Cu foil. Pyrolysis was conducted to transform the coated film into NPC. Subsequently, an MWNT film was deposited on top of the NPC film. To fabricate membranes, Cu foil was etched out, leaving NSLG/NPC/MWNT film floating on a water bath. The floating film was finally transferred to the polished nonwoven wire mesh.

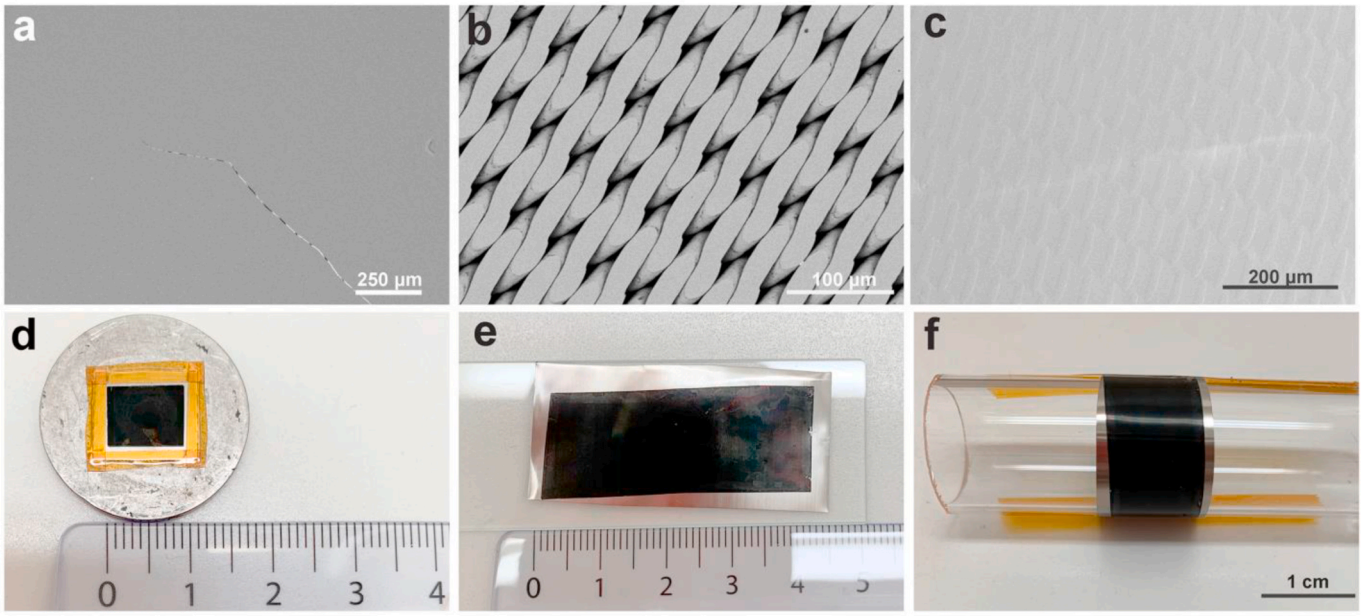

Fig. 2. Fabrication of centimeter-scale NSLG membrane on low cost macroporous support. (a) NSLG/NPC film with cracks on a conventional metal support. (b) SEM image of the commercial nonwoven stainless-steel wire mesh after manual polishing of the top surface. (c) SEM image of the transferred NSLG/NPC/MWNT film on the metal mesh. (d) Photograph of a typical all-carbon NSLG membrane suspended on the stainless-steel wire mesh. (e) Photograph of a large-area all-carbon NSLG membrane lying flat and (f) rolled up on a cylindrical tube with an outer diameter of 2.5 cm. The units of the ruler in panels (d) and (e) are in centimeter.

epoxy-based sealant. Viton rings were used to ensure a gas-tight seal between the annular disk and the membrane module. The feed and sweep gas lines were preheated and the entire membrane module was heated inside an oven with high-temperature uniformity. The gas flux was calculated once the steady-state was reached. The permeance J_i of the gas was calculated according to equation (1):

$$J_i = \frac{X_i}{A\Delta P_i} \tag{1}$$

where X_i is the flow rate of gas i, A is the membrane area, and ΔP_i is the transmembrane pressure difference for the gas i. The membrane selectivity (α_{ij}), for gas i and gas j, was calculated according to equation (2):

$$\alpha_{ij} = \frac{(C_i/C_j)_{\text{Permeate}}}{(C_i/C_j)_{\text{Feed}}} \tag{2}$$

where C_i is the concentration of gas i in a given stream.

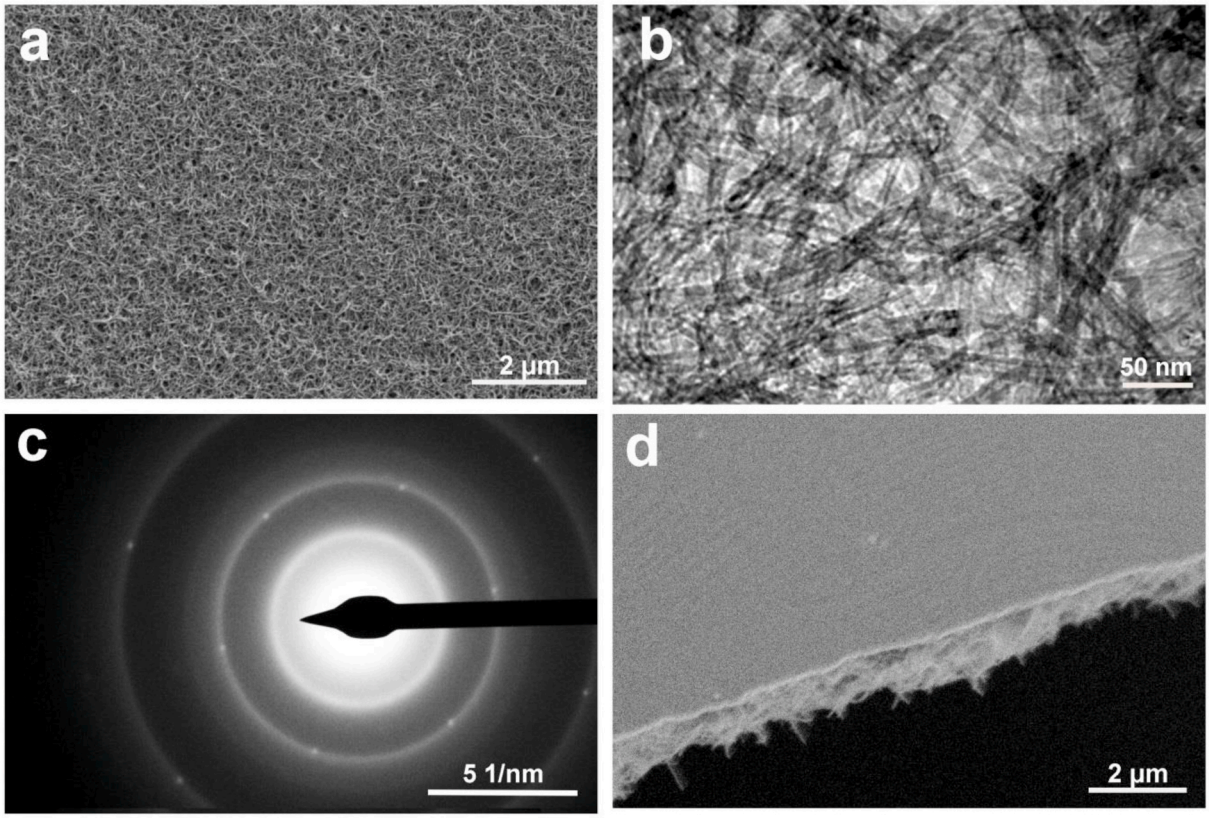

Fig. 3. Morphology of the NSLG/NPC/MWNT film. (a) Top-view SEM image of the film revealing the uniform coating of the MWNT film on top of the NPC film. (b) TEM image revealing the mesh-like structure of the MWNT film. (c) A SAED pattern from the composite NSLG/NPC/MWNT film revealing the typical diffraction pattern of graphene. (d) Cross-sectional SEM image of the flipped NSLG/NPC/MWNT film with NSLG on top.

3. Results and discussion

3.1. Fabrication of large-area graphene membrane

The procedure for preparing the reinforced NSLG membrane is shown in Fig. 1. Briefly, the NPC film, hosting 20–30-nm-sized pores (Fig. S1), was fabricated directly on top of the NSLG film using a block-copolymer based templating strategy [8]. An MWNT film was subsequently solution-cast on top of the NPC film, and the resulting composite film was annealed at 500 °C to create a good adhesion. Following this, the Cu foil beneath NSLG was removed by etching in a $Na_2S_2O_8$ bath. The resulting floating NSLG/NPC/MWNT film was rinsed with water, and finally scooped by a macroporous, nonwoven metal wire mesh leading to the suspended NSLG membrane.

The standalone NPC film without the MWNT layer works well as the reinforcing support for NSLG, however, it requires a porous support with an extremely smooth surface such as a drilled metal foil which is difficult to produce with a large area and is not economically viable for the eventual scale-up. On the other hand, when using the metal wire mesh or a conventional inorganic porous support (Fig. S2), we observed occasional cracks occurring every few millimeters in the NSLG/NPC film (Fig. 2a). This is because these supports have difficult-to-avoid occasional 1 to 10 μm-sized surface protrusions where the 100-nm-thick NPC film cracks. In this study, we overcame this obstacle by further reinforcing the graphene/NPC film with a thin MWNT layer. We chose the MWNT-based porous film as the reinforcing layer because the mesh-like carbon nanotube films have a high porosity allowing fast gas transport as well as excellent mechanical properties [28–32].

The reinforced NSLG film could be transferred to a polished nonwoven stainless-steel mesh with a pore opening of 20 μm (Fig. 2b). The suspended film was smooth and appeared to maintain its structural integrity (Fig. 2c and d). No obvious cracks or tears were observed. A few-centimeter-long coupon of NSLG/NPC/MWNT film could be prepared on the stainless-steel mesh support (Fig. 2e). A centimeter-wide film could be rolled up on a cylindrical quartz tube (2.5 cm in outer diameter) without inducing any visible cracks (Fig. 2f). This indicates that the fabrication of spiral-wound NSLG-membrane modules by this method is promising.

The morphology of the NSLG/NPC/MWNT film was analyzed by scanning electron microscopy (SEM) which confirmed that the film was free from microscale cracks (Fig. 3a). The top MWNT layer had a mesh-like structure with an interlocked array of nanotubes (Fig. 3b), similar to the carbon nanotube mesh reported in the literature [33]. This relatively open mesh-like arrangement of the nanotubes is advantageous for gas transport, enabling gas molecules to diffuse across the film with low resistance. Selected area electron diffraction (SAED) from NSLG/NPC/MWNT film transferred on a transmission electron microscope (TEM) grid with 30 μm holes revealed a characteristic diffraction pattern of SLG, representing periodicities of 0.213 and 0.123 nm, on top of the diffraction rings from nanotubes (Fig. 3c) [34]. We did not find an area in TEM grid where this characteristic diffraction pattern was not present, indicating that NSLG thoroughly adhered to the NPC/MWNT film. Flipping the composite film, we could observe the flat/smooth morphology of the NSLG film above the mesh-like structure of MWNT (Fig. 3d). The thickness of the composite film was 500 nm. We did not observe any incidence of MWNT film peeling off from the NPC film during the transfer processes, indicating a strong affinity between the MWNT and the NPC films. This is likely due to (i) strong van der Waals and π-π interaction between NPC and MWNT [8] and, (ii) potential partial penetration of MWNT tips with diameter of ca. 10 nm inside the 20–30 nm pores of the NPC film. Raman spectroscopy data, obtained from the flipped NSLG/NPC/MWNT film with graphene facing up, was

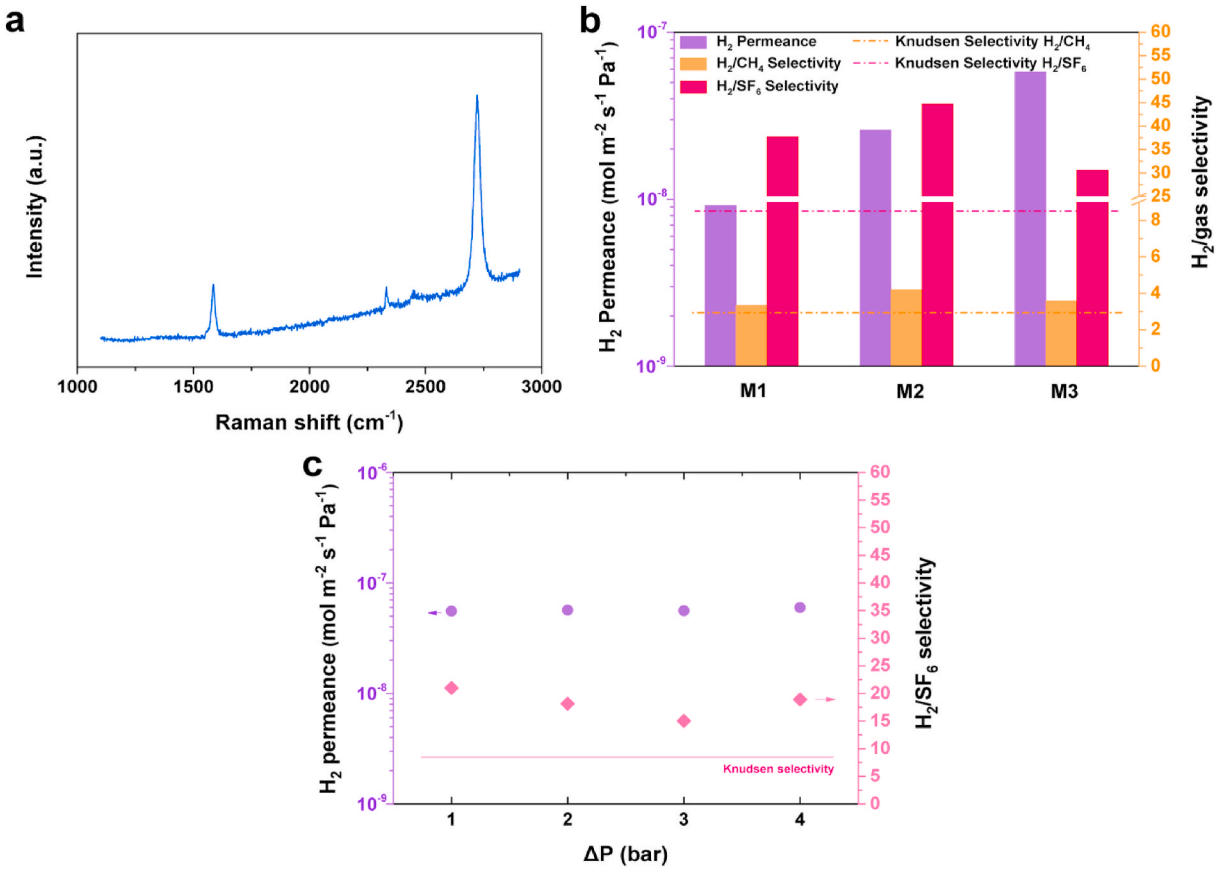

Fig. 4. Characterization of the centimeter-scale membranes prepared using the as-synthesized SLG hosting intrinsic vacancy defects (a) The Raman spectrum of SLG on Cu using a 457 nm excitation source. (b) H_2 permeance and ideal selectivities of H_2 with respect to CH_4 and SF_6 across 3 cm-scale graphene membranes (M1–M3) using a single-component feed. The horizontal dashed lines correspond to the expected Knudsen selectivity between the gas pairs when the effusive transport dominates the overall gas transport. (c) Pressure stability test of the graphene membrane (M7). H_2 permeance and H_2/SF_6 ideal selectivity as a function of trans-membrane pressure difference using a mixture feed at 25 °C.

dominated by the D and G peaks of the amorphous NPC film, and D, G and 2D peaks of the MWNT film (Fig. S3) [35,36]. Therefore, to extract information on the defect-density of NSLG, Raman spectroscopy was carried out prior to the deposition step of NPC and MWNT films (discussed later).

3.2. Crack-free centimeter-scale membranes

The gas transport and separation properties of the fabricated membrane were investigated to understand the efficacy of NPC/MWNT reinforcing layer in suppressing difficult-to-observe nanoscale cracks in the centimeter-scale membranes. For this, we first investigated the membranes prepared using the as-synthesized SLG without any further incorporation of nanopores in the graphene lattice. SLG derived from low-pressure chemical vapor deposition (LPCVD) hosts a low-density of intrinsic vacancy-defects, which could be large enough to allow gas transport. For example, SLG synthesized by LPCVD at 1000 °C using CH_4 as the carbon precursor could sieve H_2 from CH_4 with selectivity in the range of 5–13 and H_2 permeance of 5–80 $\times$ 10^{-9} mol m^{-2} s^{-1} Pa^{-1} at room temperature [8]. In this study, the as-synthesized SLG had I_D/I_G ratio of 0.08 $\pm$ 0.03, confirming that it hosted a low density of intrinsic defects (Figs. 4a and S4) [7,35].

To confirm whether the large-area membranes in this study fabricated using the as-synthesized SLG were prepared in a crack-free manner, we sealed the membranes (Fig. 2c) in a homemade module and subsequently loaded them in a gas permeation setup (Fig. S7). The feed side was pressurized to 2–5 bar while the permeate side was swept with Ar at 1 bar. We observed gas separation performance that is characteristic of a crack-free SLG membranes hosting only intrinsic vacancy defects as gas transport apertures. Three separate membranes (M1, M2, M3, M stands for membrane) were tested which yielded H_2 permeance in the range of 9–58 $\times$ 10^{-9} mol m^{-2} s^{-1} Pa^{-1} at 25 °C, similar to that reported previously from mm^2-sized membranes [8]. The low gas permeance of such membranes supported on the ultrahigh-permeance macroporous metal mesh (ca. 10^{-3} mol m^{-2} s^{-1} Pa^{-1}) support confirmed that cracks were mitigated to a large extent. The variance in the gas permeance was attributed to the batch to batch variation in the density of intrinsic defects which is difficult to control [8]. The H_2/CH_4 ideal selectivity spanned from 3.3 to 4.2, higher than that expected from the Knudsen transport (~ 2.8). These selectivities are lower than those reported from millimeter-scale membranes [8], mainly attributing to the fact that the pore-size-distribution (PSD) of the intrinsic vacancy defects is difficult to control. The H_2/SF_6 selectivity was much higher, 30–44 (Fig. 4b and Table S1), confirming that the membrane could efficiently sieve SF_6 from H_2 molecules, whose kinetic diameters are 0.55 nm and 0.29 nm, respectively. The high H_2/SF_6 selectivity established that cracks and tears were absent otherwise one would not observe the gas sieving behavior. The membranes were mechanically robust to sustain moderate transmembrane pressure of 4 bar. For example, another membrane, M7, deliberately tested for the pressure stability, could be pressurized to 5 bar on the feed side. We did not observe a change in the gas permeance as a function of pressure although a slight variation in the H_2/SF_6 selectivity (15–21) was observed (Fig. 4c). Regardless, this proves that the reinforcement of SLG with the composite carbon film allows one to prepare membranes for gas separation applications where only a moderate feed pressure is required,

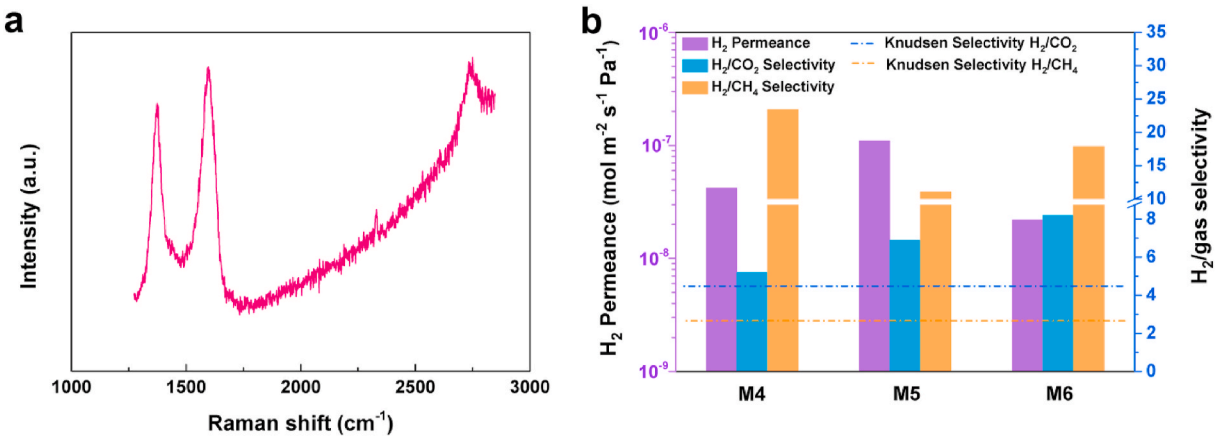

Fig. 5. Characterization of the centimeter-scale reinforced NSLG membranes prepared using the ozone-etched graphene. (a) The Raman spectrum of NSLG on Cu etched by ozone using a 457 nm excitation source. (b) H_2 permeance and ideal selectivities of H_2 with respect to CH_4 and CO_2 across three NSLG membranes (M4–M6) using a single-component feed at 100 °C. The horizontal dashed lines correspond to the expected Knudsen selectivity between the gas pairs when the effusive transport dominates the overall gas transport.

e.g., postcombustion carbon capture. The pressure loading capability of these membranes can be further increased, in principle, by choosing suitable underlying porous supports with smaller pore opening; e.g. 1–5 μm compared to 20 μm used in this study because the mechanical stress on a pressurized film scales as $D^{2/3}$ where D is the pore opening of the support [37].

3.3. Centimeter-scale NSLG membranes for H_2/CO_2 and H_2/CH_4 separation

The intrinsic defects in graphene are introduced during graphene crystallization, either as grain-boundary defects or vacancy-defects resulting from the etching of graphene by the residual O_2 in the CVD

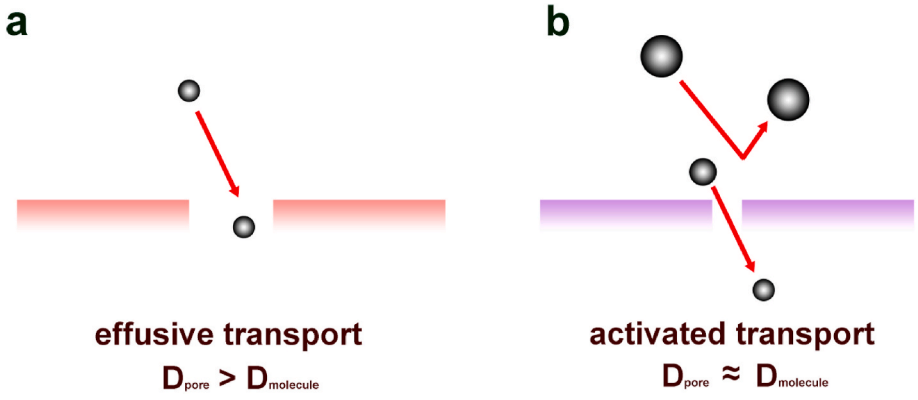

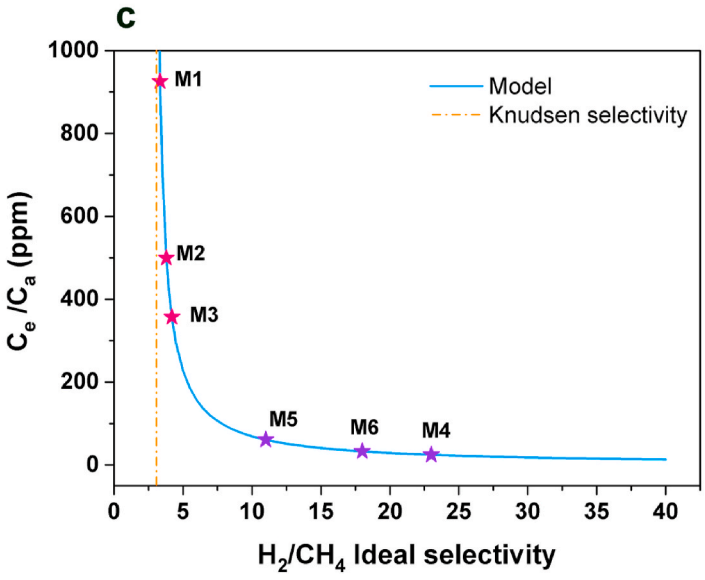

Fig. 6. Modeling the gas transport of the six NSLG membranes reported here. (a) Illustration of the effusive transport taking place in a graphene nanopore, where the pore size is larger than the gas molecule, and of (b) the activated transport, where the pore size is slightly smaller or approximately equal to the gas molecules. (c) A model that predicts the concentration of the effusive pores as a function of the measured H2/CH4 selectivity. The data from membranes M1–M6 is overlaid on top of the model. The vertical dashed line corresponds to the expected Knudsen selectivity of H2/CH4.

reactor [38]. It is difficult to control the PSD and the density of the intrinsic defects for a given separation [39–41]. Luckily, one can incorporate nanopores into SLG lattice by post-synthetic etching technique, i.e., by the ozone-based controlled etching of the graphene lattice [9]. Herein, we demonstrate that the reinforcement used in this study allows one to successfully prepare centimeter-scale H_2/CO_2 and H_2/CH_4 selective membranes.

We prepared NSLG by a controlled exposure of as-synthesized graphene to O_3 [8,9]. The etching of graphene resting on the Cu foil was confirmed by the Raman spectroscopy where I_D/I_G ratio of 0.92 could be observed (Figs. 5a and S5) [35,42–44]. Three centimeter-scale membranes (M4, M5, M6) were prepared by reinforcing NSLG with the composite carbon film and suspending them on top of the metal mesh supports. All three membranes were stable up to 130 °C, the maximum working temperature for the epoxy-based sealant used in the membrane module (Fig. S6), and yielded H_2 permeance in the range of 22–110 $\times$ 10^{-9} mol m^{-2} s^{-1} Pa^{-1} at 100 °C. The H_2 permeance and gas selectivities were similar in the single-component and gas mixture measurements for both as-synthesized as well as etched graphene membranes (Tables S3–S5). Attractive H_2/CO_2 and H_2/CH_4 selectivities of 5–8 and 11.0–23.4, respectively, could be realized from these centimeter-scale membranes (Fig. 5b and Table S2). We note that the observed H_2/CO_2 is lower than H_2/CH_4 selectivities. Since the difference between the kinetic diameters of H_2 and CO_2 is only 0.4 Å while that between H_2 and CH_4 is 0.9 Å, it is more challenging to sieve H_2 from CO_2 unless extremely precise PSD is achieved. Despite that, H_2/CO_2 and H_2/CH_4 selectivities were much higher than the corresponding Knudsen selectivities of 4.7 and 2.8, respectively, confirming once again that centimeter-scale NSLG-based gas-sieving membranes could be prepared while avoiding cracks and tears. In comparison with other reported NSLG membranes, our approach exhibits promise for the further development of the gas separation membranes based on NSLG (Table S6).

3.4. Analysis of the concentration of non-selective pores

We analyzed the gas selectivity data to understand the relative concentration of non-selective pores in the NSLG membranes reported in this study. The transport pathway of gas molecules across a two-dimensional nanopore can be classified according to the relative size of the nanopore with respect to the gas molecules. For nanopores that are slightly smaller or commensurate to the size of gas molecules, the molecules need to overcome an energy barrier, and therefore, the rate-limiting step in the overall transport is the thermal activation of gas molecules for the pore translocation. This transport regime is referred to as activated transport (Fig. 6b). For relatively bigger nanopores, the energy barrier for pore translocation is negligible, and the gas molecules can translocate the nanopores directly from the gas phase. Therefore, the permeation rates through these pores are much higher and gas molecules can directly cross the nanopores in the gas phase. This transport regime is referred to as the effusive transport (Fig. 6a). The transport rates across the graphene pores can be described by the permeation coefficient, N, which is essentially permeance per pore with the units of mol s^{-1} Pa^{-1}.

Let's consider the current case of the transport of H_2 and CH_4 through the graphene nanopores. In our model, we assumed a bimodal PSD consisting of small H_2-selective pores operating in the activated transport regime and large pores that are not selective and operate in the effusive transport regime. For simplicity, we assigned the large pore to be 2 nm in size. Choosing a higher size (e.g., 3 nm) or lower size (e.g., 1.5 nm) in this analysis will simply increase/decrease the permeation coefficient and accordingly decrease/increase the density of effusive pores. However, it would not change the relative concentration of non-selective pores from one membrane to other. In this case, the overall gas permeance can be obtained as follows [9]:

$$Permeance = C_a N_a + C_e N_e \tag{3}$$

where C_a and C_e correspond to the number of pores per unit area operating in the activated and the effusive transport regimes, respectively, and N_a and N_e are the corresponding permeation coefficients, respectively. For the effusive transport, the permeation coefficient can be obtained from the kinetic theory of gases [45]:

$$N_e = \frac{A_p}{\sqrt{2\pi m k_B T}} \tag{4}$$

where A_p is the pore area, m is the mass of the gas molecule, k_B is the Boltzmann constant, and T is the temperature. Based on this, the computed permeation coefficients of H_2 and CH_4 from a 2-nm-sized pore are 5.6×10^{-19} and 2.0×10^{-19} mol s^{-1} Pa^{-1}, respectively. The ratio of the coefficients is 2.8, which corresponds to the inverse of the square root of the ratio of corresponding molecular weights, otherwise known as the Knudsen selectivity. For the activated transport, the permeation coefficient N_a could be estimated from the translocation probability of gas molecules. This, in turn, depends on the distribution of molecular kinetic energy (Maxwell-Boltzmann distribution), where the probability to translocate is determined by the kinetic energy exceeding the energy barrier for translocation [46]. The permeation coefficient can be expressed as follows:

$$N_a = \frac{A_{eff}}{\sqrt{2\pi m k_B T}} \tag{5}$$

$$A_{eff} = \frac{1}{2} erfc\left(\sqrt{\frac{E_a}{k_B T}}\right) A_p \tag{6}$$

where A_{eff} is the effective pore area, and E_a is the activation energy of the gas molecules translocating the nanopore. We used permeation coefficients from literature where N_{a,H_2} and N_{a,CH_4} are reported to be ca. 10^{-22} and 10^{-26} mol s^{-1} Pa^{-1}, respectively, from a H_2-sieving nanopore [10,46].

The ideal selectivity, α, is simply given by

$$\alpha = \frac{Permeance_{H_2}}{Permeance_{CH_4}} \tag{7}$$

Based on this, we could calculate the ratio C_e/C_a which is given by

$$\frac{C_e}{C_a} = \frac{N_{a,H_2} - \alpha N_{a,CH_4}}{N_{e,H_2}(\alpha/2.8 - 1)} \tag{8}$$

The calculated concentration of nanopores operating in the effusive transport regime as a function of H_2/CH_4 selectivity is plotted in Fig. 6. The concentration of effusive nanopores appears to be inversely proportional to the gas selectivity for moderate selectivities (<100) mainly because of the large difference in N_{a,H_2} and N_{a,CH_4} which effectively makes equation (8) as follows:

$$\frac{C_e}{C_a} = \left(\frac{N_{a,H_2}}{N_{e,H_2}}\right) \frac{1}{(\alpha/2.8 - 1)} \tag{9}$$

Overall, the analysis predicted that all membranes in this study, with the centimeter-scale area, comprised of only a small density of effusive pores (Fig. 6c). The populations of effusive pores for membranes M1, M2, and M3 were 925, 500, and 356 ppm, respectively. The populations of effusive pores for M4, M5, M6, prepared by ozone-etched graphene were much lower (24, 60, and 32 ppm, respectively), attributing to the controlled etching of graphene by ozone [9]. This is because the introduction of new gas-sieving nanopores by the post-synthetic treatment dilutes the concentration of effusive pores with respect to the entire pore population. Nonetheless, a small concentration of effusive pores in this study validates the absence of cracks and tears in these membranes. Furthermore, the gas sieving performance from scaled-up membranes can be enhanced by diminishing the direct gas transport across graphene

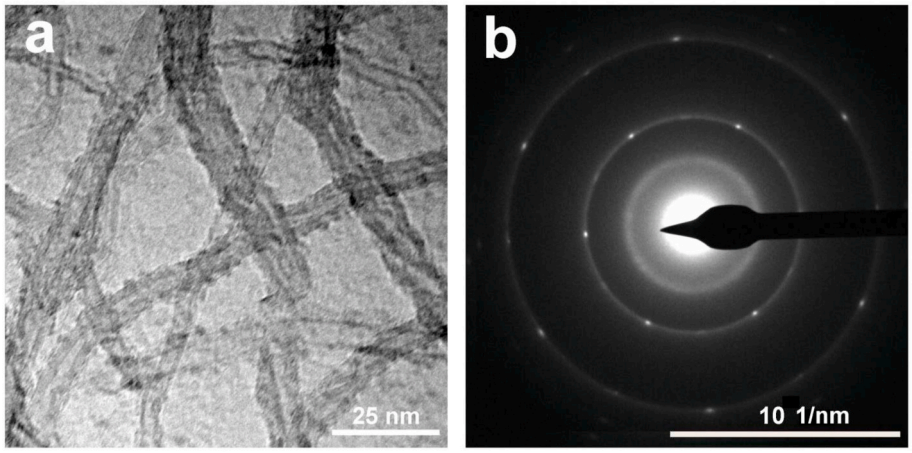

Fig. 7. Characterization of suspended NSLG reinforced solely by the MWNT film. (a) TEM image of the suspended NSLG film using only the MWNT film as the mechanical reinforcement (avoiding the NPC layer). (b) The SAED pattern from the film in (a).

nanopores, e.g., using a nanoporous polymer-based masking strategy [47].

3.5. Use of NPC-free MWNT layer to transfer graphene

Taking advantage of the potential π-π interactions between MWNT and graphene [48,49], we attempted to directly deposit the MWNT film on top of graphene for the fabrication of the reinforced NSLG membrane, avoiding the intermediate NPC layer. To understand the bonding between MWNT and NSLG, MWNT supported NSLG film was transferred to a TEM grid. Interestingly, we could also observe the characteristic SAED pattern of SLG in this case, indicating that the transfer of NSLG with MWNT was somewhat successful (Fig. 7a and b). However, the membranes fabricated from these films did not demonstrate gas sieving, and gas selectivities were lower than the corresponding Knudsen selectivities (Table S7). The H_2 permeance of MWNT-supported NSLG hosting only intrinsic defects was extremely high, 2.0×10^{-5} mol m^{-2} s^{-1} Pa^{-1}, close to that from the bare MWNT mesh (4.1×10^{-4} mol m^{-2} s^{-1} Pa^{-1}). This indicated that difficult-to-observe nanoscale cracks were indeed present in the fabricated membranes when the intermediate NPC film was not used to transfer NSLG. Using MWNT mesh, the suspended NSLG is divided into 200–300-nm-sized domains with nanotube mesh as the boundary of these domains. However, the precise control of these domains is not possible by the current method, and we speculate that occasional micron-size domains may be present in the MWNT film. Micron-size suspended NSLG is highly susceptible to mechanical failure in the pressurized environment of membranes. As discussed in the previous section, the permeation coefficient in the effusive transport regime is much higher than that in the activated transport regime; therefore, even a ppm concentration of nanoscale cracks is sufficient to deteriorate the selectivity. This underlines the important role of NPC film in preventing the cracks in NSLG membranes where the suspended domains are limited to 20–30 nm.

4. Conclusions

We report a facile and scalable fabrication route for crack-free NSLG membranes on a low-cost macroporous support with an attractive gas-sieving performance from centimeter-scale membranes. We achieved this by mechanically reinforcing graphene with a composite carbon film using a facile solution-processing method. The top layer of the composite film (MWNT layer) hosted 200–300-nm-sized pores while the bottom layer (NPC film), that contacts NSLG, had a pore size of 20–30 nm. We show that the composite film is crucial for the successful fabrication of the membrane on a low-cost macroporous support at the centimeter-scale, while the use of standalone MWNT film does not lead to the realization of gas separation which we attribute to the presence of nanoscale cracks in such films. The H_2/CH_4 and H_2/CO_2 selectivities, when analyzed by a gas transport model, indicated that the population of nanopores operating in the nonselective effusive regime was restricted to only a few ppm. Overall, the method reported here could pave the way for the further development and eventual implementation of the gas-selective graphene membranes for gas separation.

Author contributions

K.V.A. and W.L. conceived the project and wrote the manuscript. W. L. performed the experiments on graphene/NPC/MWNT membranes. L. B. and G.H. contributed to the development of graphene/MWNT films. S.H. performed the ozone treatment on graphene. M.D. performed TEM imaging. All authors contributed to revising the manuscript.

CRediT authorship contribution statement

Wan-Chi Lee: Conceptualization, Investigation, Formal analysis, Writing - review & editing. **Luc Bondaz:** Investigation. **Shiqi Huang:** Investigation. **Guangwei He:** Investigation, Formal analysis. **Mostapha Dakhchoune:** Investigation. **Kumar Varoon Agrawal:** Conceptualization, Supervision, Writing - review & editing.

Declaration of competing interest

The authors declare that they have no known competing financial interests or personal relationships that could have appeared to influence the work reported in this paper.

Acknowledgments

We acknowledge our host institute, EPFL, for the generous support. We are grateful to Swiss National Science Foundation (SNSF) AP Energy grant (PYAPP2_173645) for providing financial support for the project. W.L. would like to thank the joint EPFL-Taiwan Scholarship program for the Ph.D. grant.

Appendix A. Supplementary data

Supplementary data to this article can be found online at https://doi.org/10.1016/j.memsci.2020.118745.

References

[1] D. Jang, J.-C. Idrobo, T. Laoui, R. Karnik, Water and solute transport governed by tunable pore size distributions in nanoporous graphene membranes, ACS Nano 11 (2017) 10042–10052.

[2] P.R. Kidambi, D.D. Mariappan, N.T. Dee, A. Vyatskikh, S. Zhang, R. Karnik, A. J. Hart, A scalable route to nanoporous large-area atomically thin graphene membranes by roll-to-roll chemical vapor deposition and polymer support casting, ACS Appl. Mater. Interfaces 10 (2018) 10369–10378.

[3] Y. Yang, X. Yang, L. Liang, Y. Gao, H. Cheng, X. Li, M. Zou, R. Ma, Q. Yuan, X. Duan, Large-area graphene-nanomesh/carbon-nanotube hybrid membranes for ionic and molecular nanofiltration, Science 364 (2019) 1057–1062.

[4] S.P. Surwade, S.N. Smirnov, I.V. Vlassiouk, R.R. Unocic, G.M. Veith, S. Dai, S. M. Mahurin, Water desalination using nanoporous single-layer graphene, Nat. Nanotechnol. 10 (2015) 459–464.

[5] D. Cohen-Tanugi, J.C. Grossman, Water desalination across nanoporous graphene, Nano Lett. 12 (2012) 3602–3608.

[6] G. He, S. Huang, L.F. Villalobos, J. Zhao, M. Mensi, E. Oveisi, M. Rezaei, K. V. Agrawal, High-permeance polymer-functionalized single-layer graphene membranes that surpass the postcombustion carbon capture target, Energy Environ. Sci. 12 (2019) 3305–3312.

[7] Z. Yuan, J.D. Benck, Y. Eatmon, D. Blankschtein, M.S. Strano, Stable, temperature-dependent gas mixture permeation and separation through suspended nanoporous single-layer graphene membranes, Nano Lett. 18 (2018) 5057–5069.

[8] S. Huang, M. Dakhchoune, W. Luo, E. Oveisi, G. He, M. Rezaei, J. Zhao, D.T. L. Alexander, A. Züttel, M.S. Strano, K.V. Agrawal, Single-layer graphene membranes by crack-free transfer for gas mixture separation, Nat. Commun. 9 (2018) 2632.

[9] J. Zhao, G. He, S. Huang, L.F. Villalobos, M. Dakhchoune, H. Bassas, K.V. Agrawal, Etching gas-sieving nanopores in single-layer graphene with an angstrom precision for high-performance gas mixture separation, Sci. Adv. 5 (2019), eaav1851.

[10] S.P. Koenig, L. Wang, J. Pellegrino, J.S. Bunch, Selective molecular sieving through porous graphene, Nat. Nanotechnol. 7 (2012) 728–732.

[11] D. Jiang, V.R. Cooper, S. Dai, Porous graphene as the ultimate membrane for gas separation, Nano Lett. 9 (2009) 4019–4024.

[12] Y. Qin, Y. Hu, S. Koehler, L. Cai, J. Wen, X. Tan, W.L. Xu, Q. Sheng, X. Hou, J. Xue, M. Yu, D. Weitz, Ultrafast nanofiltration through large-area single-layered graphene membranes, ACS Appl. Mater. Interfaces 9 (2017) 9239–9244.

[13] X. Lin, P. Liu, Y. Wei, Q. Li, J. Wang, Y. Wu, C. Feng, L. Zhang, S. Fan, K. Jiang, Development of an ultra-thin film comprised of a graphene membrane and carbon nanotube vein support, Nat. Commun. 4 (2013) 2920.

[14] H. Du, J. Li, J. Zhang, G. Su, X. Li, Y. Zhao, Separation of hydrogen and nitrogen gases with porous graphene membrane, J. Phys. Chem. C 115 (2011) 23261–23266.

[15] K.V. Agrawal, L.W. Drahushuk, M.S. Strano, Observation and analysis of the Coulter effect through carbon nanotube and graphene nanopores, Philos. Trans. R. Soc. A 2060 (2016) 374.

[16] K. Celebi, J. Buchheim, R.M. Wyss, A. Droudian, P. Gasser, I. Shorubalko, J. Kye, C. Lee, H.G. Park, Atomically thin porous graphene, Science 344 (2014) 289–293.

[17] Z. Yuan, R.P. Misra, A.G. Rajan, M.S. Strano, D. Blankschtein, Analytical prediction of gas permeation through graphene nanopores of varying sizes: understanding transitions across multiple transport regimes, ACS Nano 13 (2019) 11809–11824.

[18] S. Bae, H. Kim, Y. Lee, X. Xu, J.-S. Park, Y. Zheng, J. Balakrishnan, T. Lei, H. Ri Kim, Y. Il Song, Y.-J. Kim, K.S. Kim, B. Özyilmaz, J.-H. Ahn, B.H. Hong, S. Iijima, Roll-to-roll production of 30-inch graphene films for transparent electrodes, Nat. Nanotechnol. 5 (2010) 574–578.

[19] H. Qi, Z. Li, Y. Tao, W. Zhao, K. Lin, Z. Ni, C. Jin, Y. Zhang, K. Bi, Y. Chen, Fabrication of sub-nanometer pores on graphene membrane for ion selective transport, Nanoscale 10 (2018) 5350–5357.

[20] R. Rozada, P. Solís-Fernández, J.I. Paredes, A. Martínez-Alonso, H. Ago, J.M. D. Tascón, Controlled generation of atomic vacancies in chemical vapor deposited graphene by microwave oxygen plasma, Carbon 79 (2014) 664–669.

[21] C.-K. Lee, Y. Hwangbo, S.-M. Kim, S.-K. Lee, S.-M. Lee, S.-S. Kim, K.-S. Kim, H.-J. Lee, B.-I. Choi, C.-K. Song, J.-H. Ahn, J.-H. Kim, Monatomic chemical-vapor-deposited graphene membranes bridge a half-millimeter-scale gap, ACS Nano 8 (2014) 2336–2344.

[22] K. Choi, A. Droudian, R.M. Wyss, K.-P. Schlichting, H.G. Park, Multifunctional wafer-scale graphene membranes for fast ultrafiltration and high permeation gas separation, Sci. Adv. 4 (2018), eaau0476.

[23] P.R. Kidambi, G.D. Nguyen, S. Zhang, Q. Chen, J. Kong, J. Warner, A.-P. Li, R. Karnik, Facile fabrication of large-area atomically thin membranes by direct synthesis of graphene with nanoscale porosity, Adv. Mater. 30 (2018), 1804977.

[24] L. Wang, C.M. Williams, M.S.H. Boutilier, P.R. Kidambi, R. Karnik, Single-layer graphene membranes withstand ultrahigh applied pressure, Nano Lett. 17 (2017) 3081–3088.

[25] J.W. Suk, A. Kitt, C.W. Magnuson, Y. Hao, S. Ahmed, J. An, A.K. Swan, B. B. Goldberg, R.S. Ruoff, Transfer of CVD-grown monolayer graphene onto arbitrary substrates, ACS Nano 5 (2011) 6916–6924.

[26] A.K. Nath, 9.06 - laser drilling of metallic and nonmetallic substrates, in: S. Hashmi, G.F. Batalha, C.J. Van Tyne, B. Yilbas (Eds.), Comprehensive Materials Processing, Elsevier, Oxford, 2014, pp. 115–175.

[27] D.J. Babu, G. He, J. Hao, M.T. Vahdat, P.A. Schouwink, M. Mensi, K.V. Agrawal, Restricting lattice flexibility in polycrystalline metal–organic framework membranes for carbon capture, Adv. Mater. 31 (2019), 1900855.

[28] R.S. Ruoff, J. Tersoff, D.C. Lorents, S. Subramoney, B. Chan, Radial deformation of carbon nanotubes by van der Waals forces, Nature 364 (1993) 514–516.

[29] I. Palaci, S. Fedrigo, H. Brune, C. Klinke, M. Chen, E. Riedo, Radial elasticity of multiwalled carbon nanotubes, Phys. Rev. Lett. 94 (2005), 175502.

[30] F. Fornasiero, H.G. Park, J.K. Holt, M. Stadermann, C.P. Grigoropoulos, A. Noy, O. Bakajin, Ion exclusion by sub-2-nm carbon nanotube pores, Proc. Natl. Acad. Sci. Unit. States Am. 105 (2008) 17250–17255.

[31] J.K. Holt, H.G. Park, Y. Wang, M. Stadermann, A.B. Artyukhin, C.P. Grigoropoulos, A. Noy, O. Bakajin, Fast mass transport through sub-2-nanometer carbon nanotubes, Science 312 (2006) 1034–1037.

[32] L. Yu, C. Shearer, J. Shapter, Recent development of carbon nanotube transparent conductive films, Chem. Rev. 116 (2016) 13413–13453.

[33] A. Droudian, S.K. Youn, L.A. Wehner, R.M. Wyss, M. Li, H.G. Park, Enhanced chemical separation by freestanding CNT–polyamide/imide nanofilm synthesized at the vapor–liquid interface, ACS Appl. Mater. Interfaces 10 (2018) 19305–19310.

[34] J.C. Meyer, A.K. Geim, M.I. Katsnelson, K.S. Novoselov, T.J. Booth, S. Roth, The structure of suspended graphene sheets, Nature 446 (2007) 60–63.

[35] A.C. Ferrari, D.M. Basko, Raman spectroscopy as a versatile tool for studying the properties of graphene, Nat. Nanotechnol. 8 (2013) 235–246.

[36] M.S. Dresselhaus, G. Dresselhaus, R. Saito, A. Jorio, Raman spectroscopy of carbon nanotubes, Phys. Rep. 409 (2005) 47–99.

[37] D. Cohen-Tanugi, J.C. Grossman, Mechanical strength of nanoporous graphene as a desalination membrane, Nano Lett. 14 (2014) 6171–6178.

[38] K.V. Agrawal, J.D. Benck, Z. Yuan, R.P. Misra, A. Govind Rajan, Y. Eatmon, S. Kale, X.S. Chu, D.O. Li, C. Gong, J. Warner, Q.H. Wang, D. Blankschtein, M.S. Strano, Fabrication, pressure testing, and nanopore formation of single-layer graphene membranes, J. Phys. Chem. C 121 (2017) 14312–14321.

[39] F. Banhart, J. Kotakoski, A.V. Krasheninnikov, Structural defects in graphene, ACS Nano 5 (2011) 26–41.

[40] A. Kelly, K.M. Knowles, Crystallography and Crystal Defects, second ed., J. Wiley & Sons, Ltd, 2012.

[41] M.H. Khan, M. Moradi, M. Dakhchoune, M. Rezaei, S. Huang, J. Zhao, K. V. Agrawal, Hydrogen sieving from intrinsic defects of benzene-derived single-layer graphene, Carbon 153 (2019) 458–466.

[42] L.G. Cançado, A. Jorio, E.H.M. Ferreira, F. Stavale, C.A. Achete, R.B. Capaz, M.V. O. Moutinho, A. Lombardo, T.S. Kulmala, A.C. Ferrari, Quantifying defects in graphene via Raman spectroscopy at different excitation energies, Nano Lett. 11 (2011) 3190–3196.

[43] A. Eckmann, A. Felten, A. Mishchenko, L. Britnell, R. Krupke, K.S. Novoselov, C. Casiraghi, Probing the nature of defects in graphene by Raman spectroscopy, Nano Lett. 12 (2012) 3925–3930.

[44] R. Beams, L. Gustavo Cançado, L. Novotny, Raman characterization of defects and dopants in graphene, J. Phys. Condens. Matter 27 (2015), 83002.

[45] L.W. Drahushuk, M.S. Strano, Mechanisms of gas permeation through single layer graphene membranes, Langmuir 28 (2012) 16671–16678.

[46] L. Wang, M.S.H. Boutilier, P.R. Kidambi, D. Jang, N.G. Hadjiconstantinou, R. Karnik, Fundamental transport mechanisms, fabrication and potential applications of nanoporous atomically thin membranes, Nat. Nanotechnol. 12 (2017) 509–522.

[47] G. He, S. Huang, L.F. Villalobos, M.T. Vahdat, M.D. Guiver, J. Zhao, W.-C. Lee, M. Mensi, K.V. Agrawal, Synergistic CO_2-sieving from polymer with intrinsic microporosity masking nanoporous single-layer graphene, Adv. Funct. Mater. (2020), 2003979.

[48] R. Lv, E. Cruz-Silva, M. Terrones, Building complex hybrid carbon architectures by covalent interconnections: graphene–nanotube hybrids and more, ACS Nano 8 (2014) 4061–4069.

[49] A. Saha, C. Jiang, A.A. Martí, Carbon nanotube networks on different platforms, Carbon 79 (2014) 1–18.